Research Article | Vol. 27, No. 17 | 19 Aug 2019 | OPTICS EXPRESS 24747
Optics EXPRESS

Monitoring and automatic tuning and stabilization of a 2×2 MZI optical switch for large-scale WDM switch networks

M. W. ALTAHA,[1,*] H. JAYATILLEKA,[1] Z. LU,[1] J. F. CHUNG,[1] D. CELO,[2] D. GOODWILL,[2] E. BERNIER,[2] S. MIRABBASI,[1] L. CHROSTOWSKI,[1] AND S. SHEKHAR[1]

[1] *University of British Columbia, 2332 Main Mall, Vancouver, BC, V6T1Z4, Canada*
[2] *Central Research Institute, Huawei Technologies Canada Co., Ltd, Ottawa, Canada*
[*] *altaha.mohammed@gmail.com*

Abstract: Large-scale optical switch networks employ wavelength division multiplexing to expand and facilitate multiple inputs and outputs. Such networks can be implemented with the Mach-Zehnder interferometer (MZI) as the building block. A fully-loaded MZI switch, meaning one with two optical signals at its two inputs and one that is capable of simultaneously switching those inputs to its two outputs, reduces the number building blocks within the network, and as a result makes them more power and area efficient. However, for practical operation, such MZI switches need to be automatically controlled for overcoming fabrication and thermal variations. We present an interference-based monitoring method that enables automatically switching, tuning, and stabilizing of a fully-loaded 2×2 MZI optical switch and demonstrate a prototype on an SOI platform. Using the proposed device and off-the-shelf electronics, we demonstrate automatic tuning and stabilization of an MZI switch with 12.5 Gb/s and 25 Gb/s data rates and channel spacing as small as 1 nm.

1. Introduction

Optical communication networks must address the ever-increasing demand for data. However, traditional solutions for implementing optical communication building blocks, such as modulators, switches, and filters use large area and power, and hence prevent cost-effective deployment and scaling of optical communication networks [1–3]. Silicon photonics promises to address these disadvantages by using established manufacturing techniques from the electronics industry, and enables significant area reduction in the footprint of optical devices [2,4,5]. One promising area is optical switching based on silicon photonics [4]. Optical switches enable the controllable routing of data streams from their input channels to desired output channels, in an all-optical domain without the inefficient electrical-to-optical (E/O) and optical-to-electrical (O/E) conversions required for electronic switching, as shown in Fig. 1. Several small and large-scale switch networks have been presented before [4, 6–10]. However, all of the prior-art prototypes involve switches operating only on a single-wavelength input at a given time, thereby severely limiting the scope of their practical deployment.

#356825 https://doi.org/10.1364/OE.27.024747
Journal © 2019 Received 8 Jan 2019; revised 9 May 2019; accepted 9 May 2019; published 16 Aug 2019

Optics EXPRESS

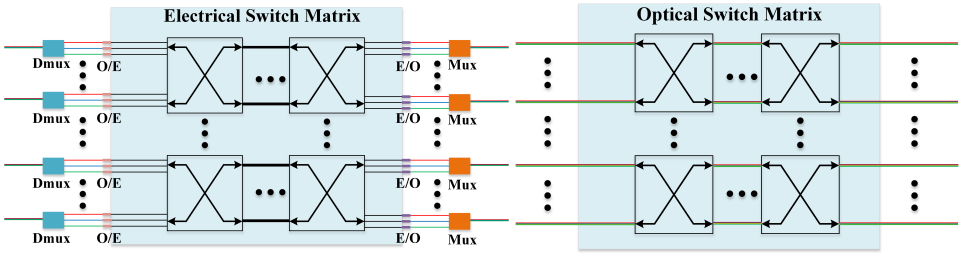

(a) (b)

Fig. 1. Switch fabric for optical communications with the switching done in (a) electrical domain and (b) optical domain.

An important building block in silicon photonics is the Mach-Zehnder interferometer (MZI), which operates on the basis of optical interference with statically or dynamically controlled phase shifting, and can be used as a modulator, a (de)multiplexer, or as an optical switch [2]. As shown in Fig. 2, an MZI can be used to switch either a single input, or two simultaneous inputs, to its outputs. When used as a switch, the MZI switch can have two desired states; bar and cross, when an input to one arm of the MZI goes out of the output arm that is in-line with it or across from it, respectively. At a perfect bar or cross state there is maximum light intensity at the desired output arm and none at the other output arm. The degree to which the MZI is being operated in the desired state is measured by the extinction ratio (ER).

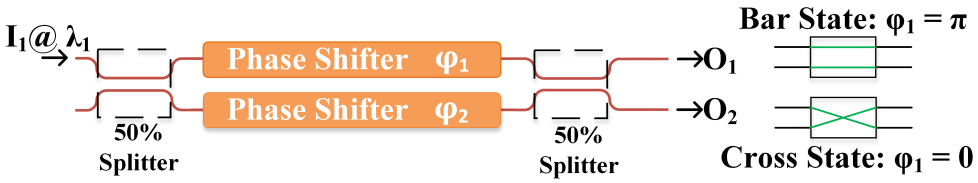

Fig. 2. Operation of 1x2 MZI optical switch.

Two main methods exist to dynamically control silicon photonics devices by tuning the refractive indices of their waveguides: 1) Thermo-optic effect: where local temperature changes are introduced to cause changes in the refractive index of silicon, and 2) electro-optic effect: where changing charge-carrier concentration in a silicon waveguide is used to change its refractive index [11].

The thermo-optic effect has an adverse side effect in that unintended changes in ambient temperature cause unintended, and often undesired, changes in device performance. Furthermore, deviation of silicon photonic waveguides from their intended dimensions due to fabrication tolerances results in uncontrolled shifts in performance metrics. Although there exist methods to desensitize silicon photonic devices to temperature variations, most of them require additional fabrication steps [12], and do not completely eliminate the problem.

One approach to address the sensitivity of silicon photonics devices to temperature variations is the use of electronic feedback techniques to constantly monitor the operating point of silicon photonics devices, and actuate them such that they are kept in their desired state [4, 11–13]. These techniques, however, need a monitoring signal that they can operate on, and for a dual-input MZI switch, providing a monitoring signal to the electronic circuit has not been possible hitherto.

Optics EXPRESS

In this paper we present a monitoring structure used in conjunction with a 2×2 MZI switch and demonstrate how it can be used to monitor and automatically tune and stabilize a dual-input MZI switch to a desired state.

The paper is organized as follows: Section II describes the need and the challenge of monitoring dual-input MZI switch. Section III presents the proposed monitoring structure and discusses its operation principle, followed by simulation results in Section IV. Section V presents static measurements depicting the operation principle. Section VI presents the tuning algorithm implemented in the controller. Sections VII and VIII present the results of two sets of measurements- static tuning and dynamic stabilization, respectively. Static tuning means automatically tuning the MZI switch to the desired state in the absence of aggressors, and dynamic stabilization means automatically tuning the switch to the desired state and keeping it there despite the effects of aggressors. Section IX presents a discussion on the proposed approach and comparison with published works. Finally, section X presents the conclusion of this work.

2. Monitoring of 1×2 and 2×2 MZI switch

As mentioned in the introduction, electronic feedback techniques can be used to place the optical switch in its desired state by monitoring the output and adjusting the switch's drive signal such that the switch remains in its desired state. This approach compensates for static effects, such as waveguide dimension deviations due to fabrication tolerances, as well as dynamic effects such as temperature drifts and thermal crosstalk.

Monitoring for a 1×2 MZI switch can be implemented as shown in Fig. 3(a) [8]. A portion of the optical power propagating in one of the MZI output arms, e.g. O_1, is tapped off and converted to an electrical current using a monitor photodiode (PD). The electronic feedback loop processes this current to determine what optimization action is needed, and adjusts the drive signal of the optical switch accordingly.

For a 1×2 MZI, this approach is sufficient because the single input to the switch is routed either to one output or to the other, so the monitoring signal, the tapped off light at one of the outputs, corresponds directly to the state of switch, and goes up and down in intensity in direct relation to the switch's state.

However, for a 2-input MZI switch, this approach does not work because as the MZI switch routes the signal of wavelength λ_1 to one output, the other output has the signal of wavelength λ_2. Thus the optical power at each output remains the same, assuming that the two inputs to the MZI at λ_1 and λ_2 have the same power and experience the same insertion loss. And since the PD is a wavelength-insensitive device, its response would be the same whether the switch is at its desired state or not, and the electronic feedback circuit could either go unstable or just lock onto a random state of the switch.

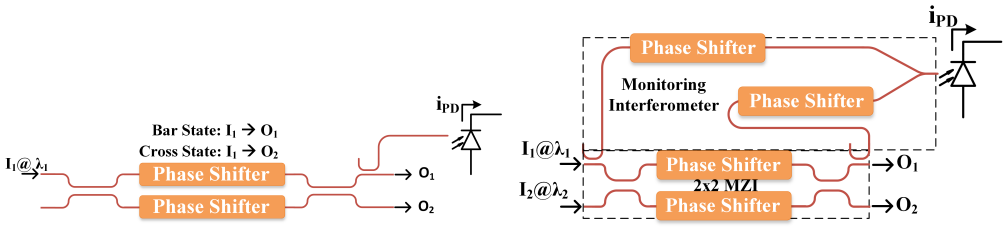

(a) (b)

Fig. 3. Monitoring structure for (a) 1×2 MZI optical switch, and (b) proposed 2×2 MZI optical switch.

Thus, a wavelength-sensitive monitoring approach is required in order to enable the implementation of an electronic feedback circuit that tunes and stabilizes a dual-input 2×2 MZI optical switch for large scale switch fabrics, without adding significant power and area penalty.

3. Proposed 2×2 monitoring structure

The concept of interference can be the basis for an approach to tune and stabilize a dual-input 2×2 MZI optical switch. Interference, the phenomenon upon which the MZI's operation is built, is inherently wavelength sensitive such that two optical signals at λ_1 and λ_2 do not interfere to produce a DC signal. Furthermore, two optical signals at the same wavelength λ_1 can only interfere if they are coherent with respect to each other, i.e., they each have a determined phase relationship [1]. In the case of coherent, same-wavelength signals, the interfering signals combine, resulting in an interference that depends on the phase difference between the interfering signals. For example, if the phase difference between two equal amplitude interfering signals I_1 and I_2 is an even (odd) multiple of π, then the resulting interference signal has a maximum (minimum) amplitude and the two waves are said to have undergone constructive (destructive) interference.

This concept is utilized in the structure shown in Fig. 3(b), where a portion of one of the inputs to the MZI is tapped off and optically combined with a tapped off portion from one of the outputs, and then the optical combination signal is terminated at the monitoring PD. The figure also shows a phase shifter in the path of the input tap that is used to control the relative phase difference between the input tap and the output tap. It can be seen that the input tap, waveguide, phase shifter, output tap, and the combiner form an interferometer that is in parallel with the main MZI – we call this the monitoring interferometer (MI).

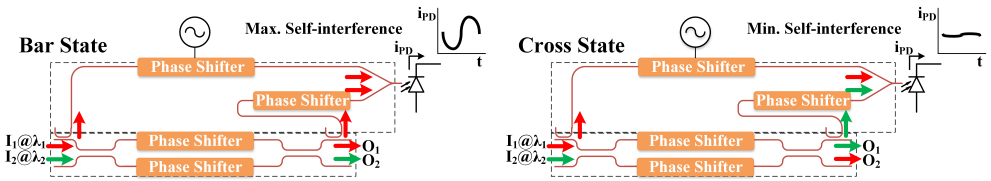

(a) (b)

Fig. 4. Operation of the proposed device in the (a) bar and (b) cross state.

To illustrate the operation of the structure, we start by assuming that the MZI switch is operating in the bar state (Fig. 4(a)). In this case, both inputs to the MI are at same wavelength since very little optical power from λ_1 is routed to output arm O_2.

The initial phase difference between the two inputs to the MI cannot be predicted ahead of time because it is wavelength and geometry/layout dependent and also because it itself can vary due to the same effects that can adversely affect the performance of the MZI switch which we are trying to compensate for. However, if the phase shifter in the MI is excited with a periodic signal of such an amplitude that the resulting phase change to the input tap signal is 2π, then we are guaranteed that the output optical signal of the MI goes through a point of constructive interference and a point of destructive interference, at twice the frequency of excitation as the MI's phase shifter. And since the switch is in the bar state, the interference points are at their strongest levels, constructive or destructive, since the tapped off light from the output O_1 of the MZI consists largely of the same wavelength as the light in the other arm of the MI (tapped at I_1).

Conversely, when the MZI is in the cross state (Fig. 4(b)), the second input to the MI contains very little optical signal at the same wavelength as that in the first input of the MI, and hence no interference can occur. Thus, the MI's output goes through zero or minimal variations if the phase shifter of the MI introduces minimal losses.

Optics EXPRESS

As the output of the MI is terminated at the PD, therefore, its output current also goes through the same periodic strong or minimal variations for bar or cross state, respectively. Hence the monitoring signal that indicates the state of the MZI switch is the swing amplitude of the PD's output current instead of the the absolute or average value of this output current. This swing amplitude is at its largest (smallest) value at the bar (cross) state because of the strong (lack of) constructive and destructive interference patterns.

4. Simulation of the proposed device

An MZI switch with the proposed monitoring structure is simulated using Lumerical INTERCONNECT. The voltage to the main MZI switch's phase shifter is linearly swept while the phase shifter of the MI is excited with a periodic signal. The outputs of both MZI arms and the output of the MI are monitored for optical power and wavelength composition (spectrum).

Figures 5(a) and 5(b) show the spectrum of the bar and cross outputs of the main MZI, respectively. In Fig. 5(a), the bar state occurs at around 2.05 V and causes the 1550 nm wavelength to be maximized at the through port and the 1540 nm wavelength minimized. Conversely, the cross state occurs at a drive voltage of around 3 V and causes the 1540 nm wavelength to be maximized at the through port and the 1550 nm wavelength minimized. In Fig. 5(b), the opposite order occurs for the cross port. In Fig. 5(a), the difference in optical power between the 1540 nm signal at the bar state and the 1550 nm signal at the cross state is caused by the simulation model only including the optical taps for the MI, which affect only one of the MZI's input arms and one of its output arms, and as a result these optical signals have power imbalance going into the MZI switch. The fabricated switch, for which the measurement result are presented in the coming sections, included dummy taps for the other arms of the MZI switch to equalize the power loss between the inputs and outputs.

Figure 5(c) shows the output of the MI while the MZI's state is being swept, where it can be seen that the AC amplitude of the signal at 1550 nm wavelength is maximized (even if its average value isn't) at the bar state of the switch and minimized at the cross state of the switch, respectively.

After confirming the viability of the operation principle of the proposed monitoring approach through simulations, we demonstrate measurement results of fabricated devices embodying the proposed approach in the next sections.

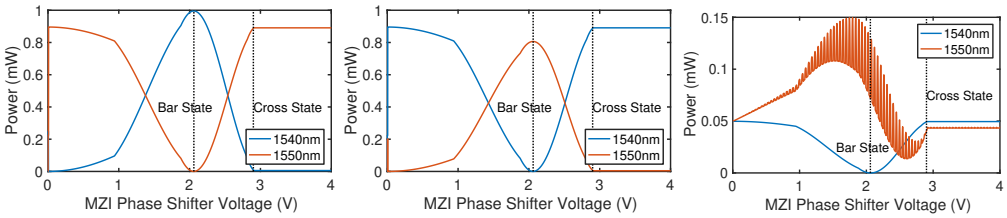

Fig. 5. Optical output of (a) MZI bar arm, (b) MZI cross arm, and (c) MI, as the MZI phase shifter is swept, along with a periodic excitation signal applied to the MI's phase shifter.

Optics EXPRESS

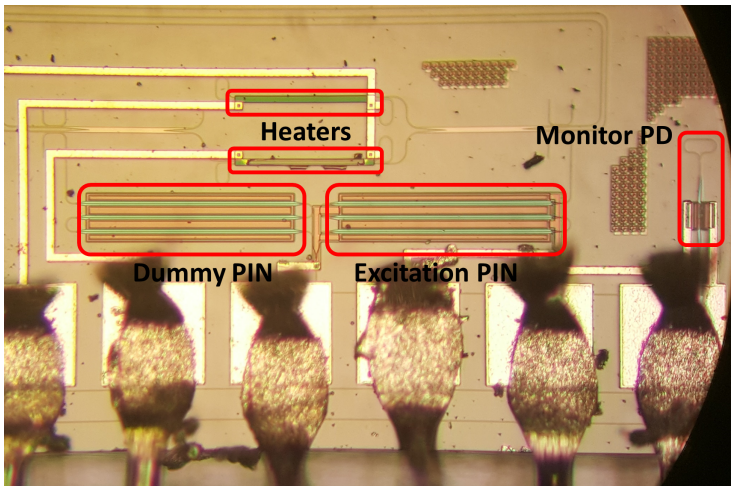

Fig. 6. Micrograph of fabricated device.

5. Measurement setup and static characterization

5.1. Device under test

A micrograph of the MZI-MI device fabricated in IME silicon photonics process is shown in Fig. 6. The device has seven pads; three pads for the two thermal phase shifters of the main MZI, labelled "heaters" in the figure (one of these pads is not visible in the figure because the micrograph is cropped to show more of the switch's area), two pads for the MI's PIN phase shifter, labelled "Excitation PIN" in the figure, and two pads for the on-chip PD. A "Dummy PIN" is placed in the MI's second arm for the purpose of having both MI arms balanced (in terms of propagation distance and loss) when no signal is applied to the excitation PIN. The photonic integrated circuit chip was placed on a breakout PCB and wirebonded to PCB pads. The footprint of the fabricated device, including the MI, monitoring PD, and electrical pads, is about 270 μm $\times$ 684 μm.

5.2. Static measurements

The MI's phase shifter is driven with a function generator with an output impedance of Z_s. Since the phase shifter is a PIN diode, the impedance seen by the function generator varies from a high impedance ($> Z_s$), when the PIN diode is still off, to a low impedance ($\leq Z_s$) as the PIN diode turns ON and becomes forward biased. Thus the amplitude of the function generator's output is set to be higher than the actual swing that would be seen across the phase shifter.

The MZI's inputs are provided by either an Agilent 81682A programmable laser or a Keysight N7714A high power laser, and the outputs are connected to Agilent 81635A optical-power detector modules. Both the lasers and detectors are controllable using a GPIB-connected PC.

Figure 7 shows the setup used to characterize the switching spectrum of the MZI-MI structure. The PC controls two dual-channel Keithley 2602A source-measure units (SMU). One channel is used to sweep the drive to one of the MZI's thermal phase shifters, another channel is used to sweep the drive to the MI's PIN phase shifter, and a third channel is used to read the output current of the monitor PD.

As the switching transfer curve for an MZI is linear with respect to the power dissipated in its thermal phase shifter (within the linear region), the MZI's phase shifter drive is incremented in the power domain instead of the current or voltage domain. This is achieved by incrementing the voltage across the heater, reading the current drawn by the respective SMU channel, and

Optics EXPRESS

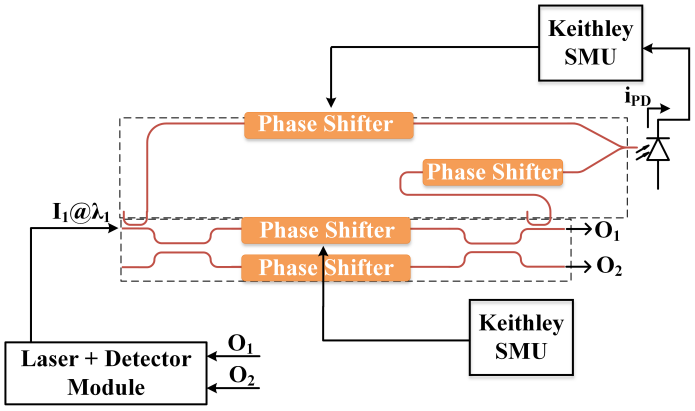

Fig. 7. Test setup for switching spectrum characterization.

calculating the new power dissipated in the heater. Once a certain power increment is achieved, the phase shifter's drive, the measured optical power at the output of the MZI as well as the current output of the monitor PD are recorded.

While this test is running, a nested loop is also executed which controls the SMU channel connected to the MI's PIN phase shifter. As the turn-on voltage for the PIN phase shifter is measured to be 0.7-0.8 V, the nested loop is programmed to start at 0.5 V and increment with fine voltage steps (since small voltage increments result in large current increments when the PIN diode is in the forward bias region). This nested loop reads the current sourced from the SMU channel at each voltage point and also the monitor PD's output current.

Consequently, for each point on the MZI's switching spectrum, a full set of data is obtained for the MI's phase shifter's voltage and current, as well as the PD's output current. This latter set of data captures the extent of interference at the output of the MI. The resulting plot is shown in Fig. 8 where the blue and green curves show the MZI switch's outputs as a function of the electrical power supplied to the thermal phase shifter. The red curve shows the monitor PD's output current swing at each point on the MZI's switching spectrum as calculated from the data gathered by the nested loop. It can be seen from Fig. 8 that the the maximum (minimum) PD output current swing coincides with the bar (cross) state of the MZI switch.

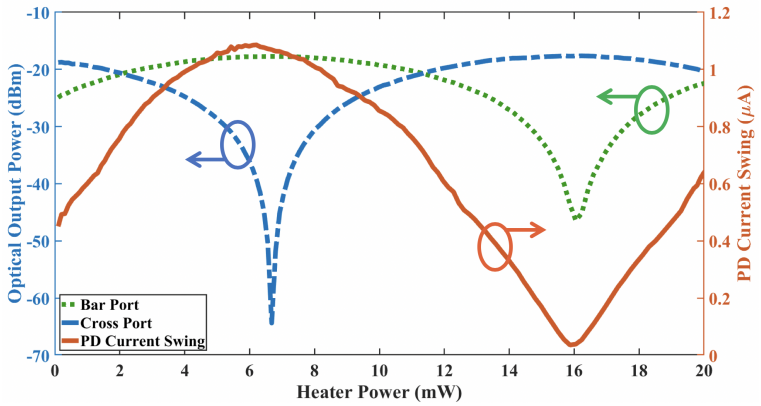

Fig. 8. Experimental switching spectrum of the MZI switch and the monitor PD current swing at λ=1550 nm.

Optics EXPRESS

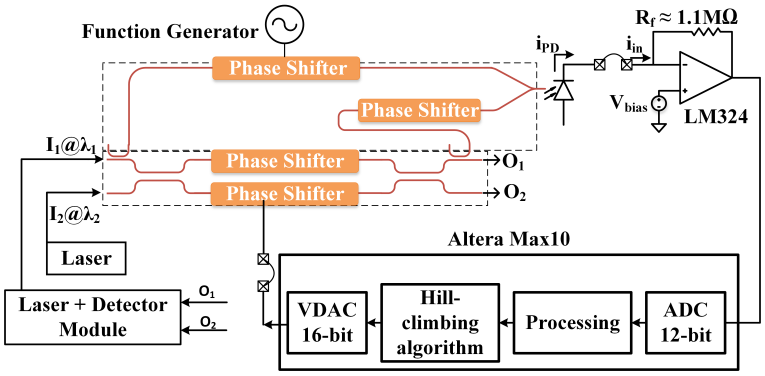

Fig. 9. Proposed MZI-MI switch with an electronic control loop.

5.3. *Open-loop measurement*

The electronic feedback loop is assembled using off-the-shelf components and an FPGA board, as shown in Fig. 9. The monitor PD's current is converted to a voltage signal and amplified using a transimpedance amplifier (TIA) built from an opamp IC with a shunt-feedback resistor. The TIA output is connected to the FPGA's on-chip analog-to-digital converter (ADC). The FPGA then processes the ADC's output signal, implements the tuning algorithm, and determines the corresponding drive voltage to the MZI's heater. This value is then sent to an on-board voltage-output digital-to-analog converter (DAC) that is connected to one of the MZI's heaters' pads (signal and common ground). According to [6], a voltage-output DAC (VDAC) would be superior to a current-mode DAC when the thermal variations are taken into consideration.

For open loop measurements, the MI's PIN phase shifter is driven with a function generator at 1 kHz and with an amplitude enough to vary the voltage across the PIN diode from 0.5 V - 1.2 V. The cathode of the monitor PD is connected to the TIA, and the output of the TIA is viewed with an oscilloscope. The MZI heater's drive is varied and the TIA output is captured on the oscilloscope at the bar and cross states. Figure 10 shows the oscilloscope capture of the PIN phase shifter's excitation and TIA output signals near the bar and cross states of the MZI, demonstrating that the swing amplitude of the monitor PD's output current is indicative of the state of the MZI switch.

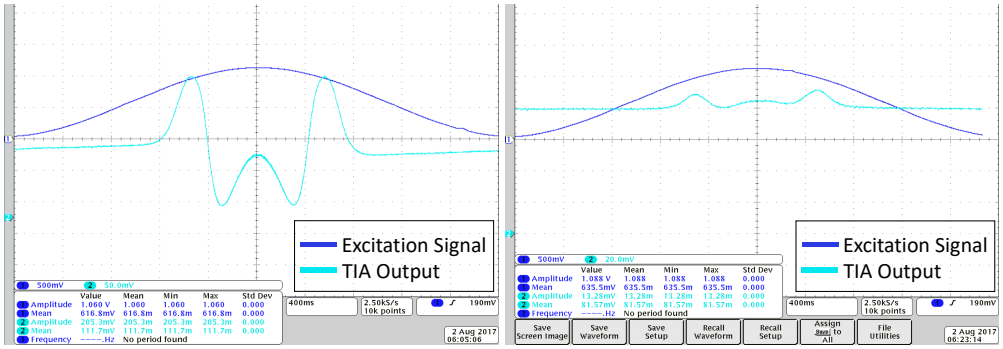

(a) (b)

Fig. 10. Oscilloscope capture of the MI's phase-shifter's excitation signal and the TIA output at the MZI's (a) bar and (b) cross state.

Optics EXPRESS

6. Automatic tuning algorithm

The tuning algorithm needs to be able to tune the optical switch to the desired state and keep it there, until the operator decides to change the state, despite any adverse effects. Two key factors drove the formulation of the tuning algorithm: 1) the optical power coming into the photonic integrated-circuit containing the switch fabric, and 2) minimizing the number of possible inputs since our target application is a large optical switch fabric, and each extra input to the tuning algorithm may result in extra pins/pads. Thus, a blind, automatic tuning algorithm is needed. By blind we imply that the tuning algorithm should operate independently of the input optical power level, which means that the fluctuations in the input laser's power are transparent to the algorithm. Furthermore, the algorithm should operate without a need for an external reference; an output level that is considered as meeting the desired performance of the switch in its current state.

With the switching characteristic of the MZI switch containing a single global peak within one period, with monotonicity on either sides of the peak, a preturb-and-observe approach, [14], is used to implement a hill-climbing, or a maximum-point seeking algorithm is used for tuning. The algorithm perturbs the bias point of the MZI switch, and from the observed response it determines whether the current operating point of the switch lies on a region of positive slope or negative slope of the transfer function. A caveat here is that the positive and negative slopes in this context are relative to the excitation direction. For example if the initial operating point of the switch is to the right of the peak and the control loop perturbs this operating point to the right, then the observed response looks like a negative slope response. Conversely, if the control loop excites this operating point to the left, then the observed response looks like a positive slope response. In both cases, the tuning algorithm drives the control loop to move the operating point in the direction of the positive slope, hence the hill-climbing behavior.

With this approach, the control loop is constantly looking for a peak, which also means that the loop is constantly compensating for variations in the input optical power and any dynamic effects that might adversely effect the switch's operating point, such as thermal crosstalk.

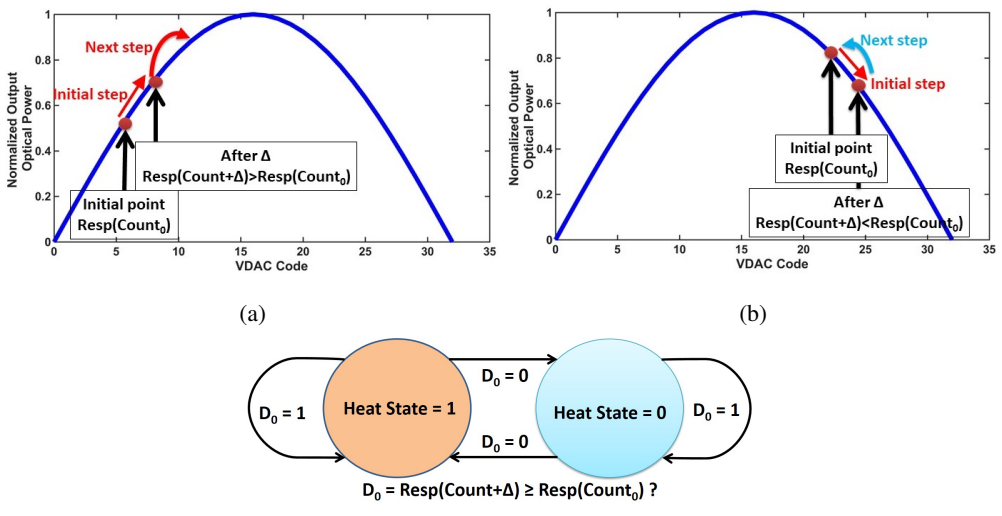

Fig. 11. Illustration of automatic tuning algorithm on (a) positive slope, and (b) negative slope. (c) state diagram of the tuning algorithm.

Optics EXPRESS

Admittedly, one disadvantage of this approach is that the tuning algorithm is also blind to the exact location of the peak and that the control loop would keep overshooting the peak until it detects a slope-reversal condition. This behavior may result in some eye closure as the output of the control loop is sometimes off the optimum value. However, this effect can be mitigated if the tuning algorithm is combined with additional states that turn tuning ON/OFF at specific times.

Figure 11 illustrates the operation of the tuning algorithm, wherein, a half period of a raised cosine function representing the output intensity of an MZI's output is plotted versus a driving DAC output code. A 5-bit DAC sufficient to entirely cover the half period of the raised cosine function is assumed. Figure 11(a) shows the scenario where the algorithm's initial position lies to the left of the peak. The algorithm records the response of the switch, Resp($Count_0$), and takes a first step towards increasing VDAC code. The algorithm then records the new response of the MZI switch, Resp($Count_0 + \Delta$), and compares the two values, and since the new value is greater than the initial response value, the algorithm knows that it is moving on a positive slope, and keeps increasing the VDAC code. Figure 11(b) shows the case where the algorithm detects it is moving on a negative slope (red arrow), and decides to reverse its climb direction (blue arrow). Figure 11(c) shows that the algorithm can be described with only two states, meaning that a single-bit control is sufficient. Lastly, It is worth mentioning that the step size in an actual system can be manipulated to achieve desired metrics such as speed and accuracy, limited by the front-end electronics that feed the controller.

As mentioned above that an important feature of the tuning algorithm is compensation of fluctuations in the input optical power. It can be seen from the description of the operation of the algorithm, as well as from the scenarios depicted in Figs. 11(a) and 11(b), and the state machine depicted in Fig. 11(c) that fluctuations in the input optical power look like perturbations to the MZI switch's operating point, and hence the algorithm would compensate for them.

Next, we describe the setup and results of the closed-loop measurements done on the MZI-MI structure with the controller automatically tuning the MZI switch to the desired state.

7. Closed loop static tuning with two simultaneous input wavelengths

With the control loop closed, we carry two types of measurements- static tuning and dynamic stabilization. In static tuning measurements, the control loop tunes the MZI switch to the desired state in the absence of any aggressor signal. This section presents the results for closed-loop static tuning measurements with two simultaneous input wavelengths.

The MZI switch has two optical inputs, I_1 at λ_1 and I_2 at λ_2. Since the power detectors to which the MZI's outputs are connected are wavelength-insensitive, there is no way of knowing whether the tuning loop is working properly, as the power read by the detectors would not indicate the wavelength composition. Therefore, optical filters are placed in between the outputs of the MZI and the power detectors so as to discern the power of each optical signal at each of the outputs of the MZI by tuning the filters to that signal's wavelength.

Figure 12 demonstrates the results for using the controller to automatically tune the switch to the desired state for either inputs. During this test the fiber array is aligned such that the peak transmission wavelength of the input/output grating couplers to the MZI switch is around 1530 nm. The two input wavelengths are chosen as 1525 nm for I_1 and 1530 nm for I_2 to demonstrate that the monitoring approach works with channel spacing as low as 5 nm. Then the control loop is run twice for three minutes, with the PC recording the power meter readings at one second intervals each time. During the first minute the output voltage of the controller is 0 V. Then at the one-minute mark the controller starts working to place the switch in the bar state. At the two-minute mark the controller is set to tune the switch to the cross state. Finally at the end of the three minutes the PC program stops the capture. The first time this test is done, the filters are set to λ_1, and the loop correctly tunes to the desired state at each of intervals where the controller is working. The second time the test is run the filters are centered at λ_2.

Optics EXPRESS

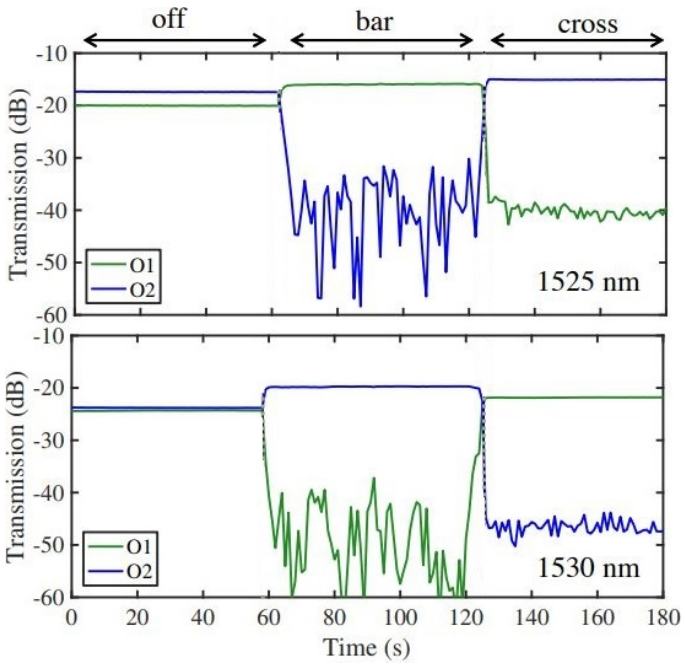

Fig. 12. Power at the MZI's output arms with two simultaneous inputs; I_1 at 1525 nm and I_2 at 1530 nm. Inserts at bottom-right corners indicate the center wavelength of the optical filters between MZI and power detectors. Controller is effectively off for the first minute, then tunes to the bar state for a minute, then tunes to cross state for a minute.

Next, the optical signals at I_1 and I_2 are modulated to evaluate if the automatic tuning circuit tunes the MZI switch so that the data from each signal appears at the desired output without corruption. We should note that in preparing for this set of measurements, we modified the fiber array angle such that the peak transmission of the input and output grating couplers was around 1550 nm. With this new alignment, we also wanted to demonstrate that the proposed monitoring approach and control loop work for smaller channel spacing. Thus, we chose our input wavelengths as λ_1 = 1550 nm and λ_2 = 1549 nm.

The optical signals are first passed through external modulators driven by pulse-pattern generators (PPGs) before they are fed to the inputs of the MZI switch as I_1 and I_2. One of the PPGs is limited to 12.5 Gb/s, so we started the measurements with both inputs set to 12.5 Gb/s, then added a set of measurements with the other PPG's data rate set to 25 Gb/s. Additionally, PRBS31-pattern is chosen in order to show that the controller is not sensitive to the long consecutive identical digits (CIDs) of 0s and 1s. Depending on the optical signal which is being tuned by the controller to a given state, one of the outputs of the switch is then connected to an EDFA amplifier followed by a variable optical attenuator to bring the optical signal level to power levels suitable for the optical receiver.

A Discovery Semiconductor optical receiver (DSC-R411-69-FC/PC-K-2) is used to convert the optical signal to a high-speed electrical output, which is then sampled by a sampling oscilloscope to obtain the eye diagram. To compare the performance of the control algorithm and the automatic controller, measurements are also done by disconnecting the controller from the MZI's phase shifter and manually tuning the switch to the desired state and obtaining an eye diagram.

In the first case, output arm O_1 of the MZI switch was connected to the optical receiver. In this configuration when the switch is tuned to the bar state, the data of signal I_1 appears at O_1 of the switch, and when tuned to the cross state, the data of signal I_2 appears at O_1 of the switch.

Optics EXPRESS

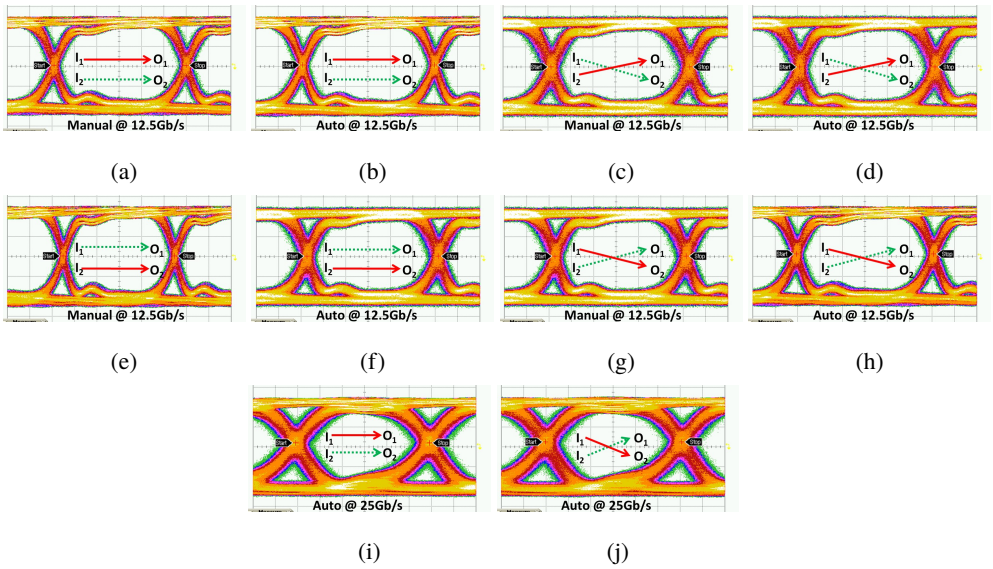

Fig. 13. Eye diagrams at the output of the switch under different tuning conditions with two optical-signal inputs that are simultaneously and independently modulated: 12.5 Gb/s I_1 at O_1 port with (a) manual and (b) automatic tuning to the bar state, respectively. 12.5 Gb/s I_2 at O_1 port with (c) manual and (d) automatic tuning to the cross state, respectively. 12.5 Gb/s I_2 at O_2 port with (e) manual and (f) automatic tuning to the bar state. 12.5 Gb/s I_1 at O_2 port with (g) manual and (h) automatic tuning to the cross state, respectively. 25 Gb/s I_1 with automatic tuning at (i) O_1 port in bar state, and (j) O_2 port in cross state. I_1 has λ_1=1550 nm, I_2 has λ_2=1549 nm. Measured eye heights are 165 mV and 127 mV at 12.5 and 25 Gb/s, respectively.

Figures 13(a) and 13(b) show the eye diagram of signal I_1 with manual and automatic control to tune the switch to the bar state. Figures 13(c) and 13(d) show the eye diagram of signal I_2 with manual and automatic control to tune the switch to the cross state.

Next, the optical receiver is connected to the output arm O_2 of the switch, and measurements are repeated for both cases: 1) manually, and then automatically, placing the switch in the bar state such that the data of signal I_2 appears at O_2 as shown in Fig. 13(e) and 13(f), respectively, and 2) manually, and then automatically, placing the switch in the cross state such that the data of signal I_1 appears at O_2 as shown in Fig. 13(g) and 13(h), respectively.

As one of the PPGs can support 25 Gb/s, measurements with one of the PPGs outputting data at 25 Gb/s and the other one at 12.5 Gb/s are also carried out. Figure 13(i) and 13(j) show the eye diagram for 25 Gb/s data on I_1 in the O_1 arm and in the O_2 arm of the switch with controller automatically tuning the switch to the bar state and cross state, respectively.

Finally, as noted in the caption of Fig. 13, the measured eye heights are around 165 mV for the 12.5 Gb/s measurements, and around 127 mV for the 25 Gb/s measurements, which demonstrates how little of a penalty to vertical eye closure is induced by the controller. And since the time scale on the eye diagrams is almost identical, it can be seen that there is almost no penalty to horizontal eye closure induced by the controller.

Optics EXPRESS

8. Closed loop dynamic stabilization with two simultaneous input wavelengths

As mentioned earlier, optical switches also need to be stabilized against active, dynamic aggressor effects resulting from the switching crosstalk [7, 15–17] from nearby elements. Thus to demonstrate the ability of the control loop to stabilize the switch state against dynamic effects, an aggressor signal is introduced on the second phase shifter of the main MZI. The amplitude of this aggressor signal is chosen such that it would completely take the switch out of a perfect state. To this end, the switch is first manually placed in the best bar state achievable by manually adjusting the output voltage of one channel of an SMU to control one of the thermal phase shifters of the main MZI, the same phase shifter that the controller would later actuate. This process is what we will refer to henceforth as manual tuning. Another channel of the SMU is used to gradually increase the drive to the other phase shifter while monitoring the power read by the power meters. It is found that 1.2 V is sufficient to take the switch out of the best bar state achievable, and even partially reverse the optical power routing. This operation is then repeated by first placing the switch in the desired state, then ramping the drive voltage to the second phase shifter to 1.2 V in one minute, then ramping it down back to 0 V in one minute.

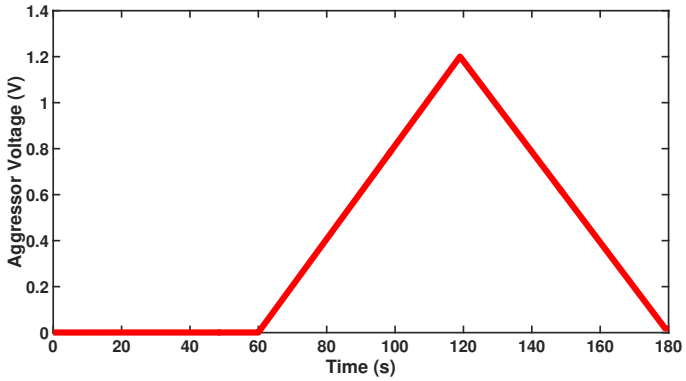

Fig. 14. Aggressor waveform.

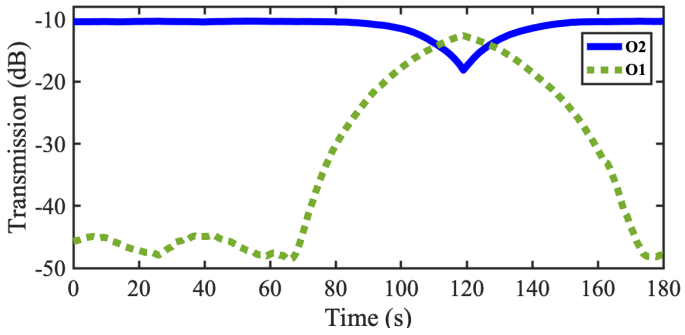

Fig. 15. Effect of the aggressor signal on the best achievable, manually tuned, bar state of MZI switch.

Optics EXPRESS

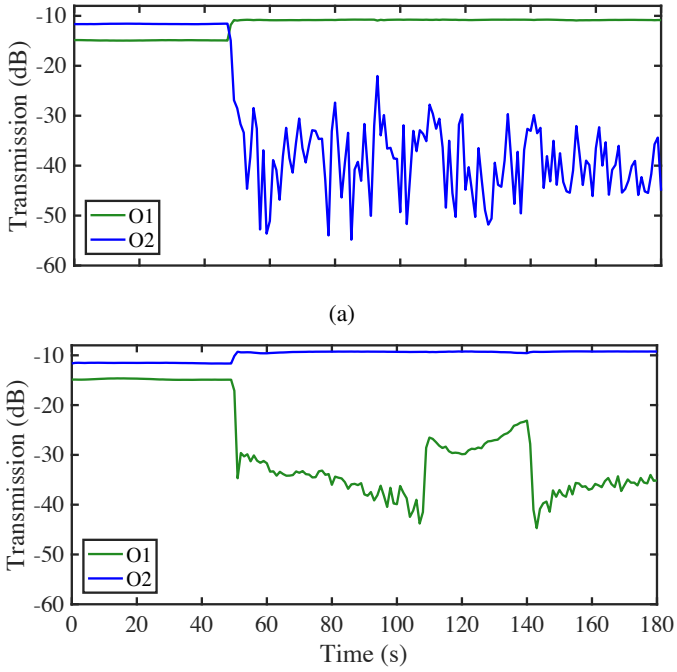

Fig. 16. Power at the output ports of the MZI switch with the filters centered at λ_1 = 1550 nm and the controller tuning the switch and stabilizing it against the aggressor signal: Switch tuned to the (a) bar state where λ_1 is routed to the O_1 port and (b) cross state where λ_1 is routed to the O_2 port.

Figure 14 shows the aggressor waveform and Fig. 15 shows its effect on the state of the switch. This aggressor signal is then programmed into the PC with a period of one minute preceding it where no aggressor signal is applied. During the first 45 seconds, the controller is off, then at the 45-second mark the controller is turned ON and allowed to tune the switch to the bar state before the aggressor signal starts ramping up. During this test the optical filters are set to λ_1. The test is repeated a second time but with the controller turned ON and programmed to tune the switch to the cross state. These two tests are then repeated while the filters at the output of the switch set to λ_2. Figure 16(a) and 16(b) show these tests, respectively.

Two things are worth commenting on in Fig. 16; first is the seemingly large ripples on the cross port output in Fig. 16(a), it can be seen from Fig. 8 that in the bar state, which is around 6.5 mW, the cross port output has a steep slope such that any perturbation to the MZI's state result in large variations on this port. These variations could have a negative effect on the next switch since they could eventually appear as noise to the next switch's controller. This possibility depends on whether the variations have significant amplitude after going through the optical taps and TIA of the next switch's controller. Second, it is noticeable that in (b), the O_1 output undergoes a jump to higher power level around the 110 seconds mark and stays there until around the 140 seconds mark. We noticed that during the test, the output of the controller kept increasing to offset the effect of the aggressor signal, until the output of the controller reached the supply limit of the on-board output DAC. The controller is programmed such that if this scenario were to happen, i.e. if the digital value of the controller's output reached its maximum value, then the controller is to resume the searching from lower output value.

Optics EXPRESS

This switching to a lower output value is what occurred during this test and resulted in the controller switching its searching range and resuming the tuning action within that new range. This behavior was observed by connecting a voltmeter to the output of the DAC and observing the value of this output. Due to the unavailability of a data acquisition (DAQ) capability, we can not present this behavior of the controller's output.

As with the static tuning results in the previous section, the performance of dynamic stabilization of the controller with data transmitted on the input signals I_1 and I_2 are evaluated next.

In the first set of measurements, I_1 and I_2 are connected to the input arms 1 and 2, respectively, and the optical receiver chain is connected to the output arm O_1 of the switch. Thus, in the bar state, I_1 appears at the O_1 port and at the cross state I_2 appears at the O_1 port. First, the switch is manually placed in the bar state and the eye diagram is captured. Then the aggressor signal is introduced and the measurement is repeated with the controller turned ON. The controller is allowed to tune the switch to the bar state during the one-minute period when the aggressor signal is inactive, later followed by five periods of up and down ramps of the aggressor signal. Figure 17(a) shows the eye diagram with the switch manually tuned, and Fig. 17(b) shows the eye diagram for automatic tuning and stabilization. The same tests are repeated for the cross state where Fig. 17(c) shows the eye diagram of signal I_2 at the O_1 port when the switch is manually tuned to the cross state with aggressor, and Fig. 17(d) shows the eye diagram when the controller is automatically tuning the switch to the cross state and stabilizing the switch against the aggressor.

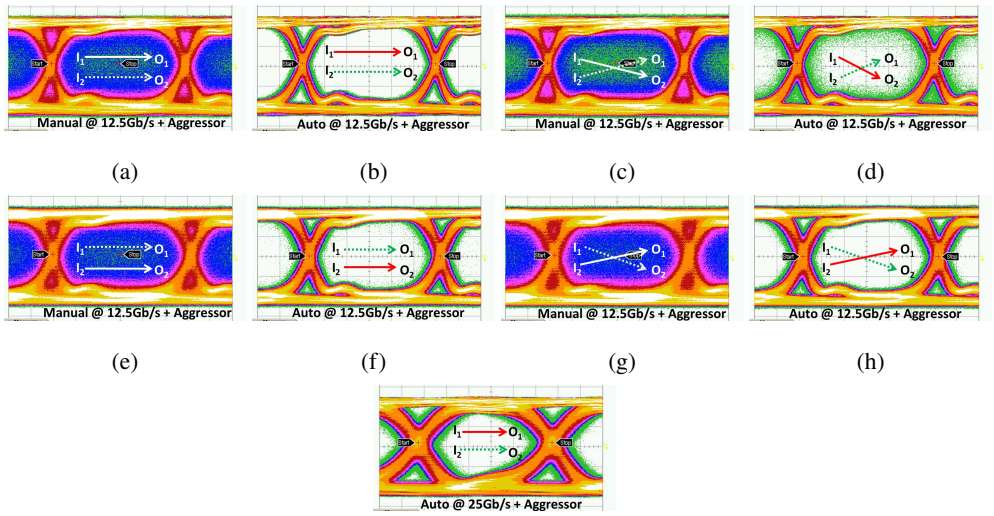

Fig. 17. Eye diagrams at the output of the switch under different tuning and stabilization conditions with 5 periods of the aggressor signal of Fig. 14 and two optical inputs that are simultaneously and independently modulated: 12.5 Gb/s I_1 at O_1 port with (a) manual tuning and (b) automatic tuning & stabilization to the bar state, 12.5 Gb/s I_1 at O_2 port with (c) manual and (d) automatic tuning & stabilization to the cross state, 12.5 Gb/s I_2 at O_2 port with (e) manual and (f) automatic tuning & stabilization to the bar state, 12.5 Gb/s I_2 at O_1 port with (g) manual and (h) automatic tuning & stabilization to the cross state, (i) 25 Gb/s I_1 at the O_1 port with automatic tuning & stabilization to the bar state. I_1 has λ_1=1550 nm, I_2 has λ_2=1549 nm. Measured eye heights are 165 mV and 127 mV at 12.5 and 25 Gb/s, respectively.

Optics EXPRESS

Next, the optical receiver is then connected to the O_2 port such that the data of I_2 and I_1 appear at the receiver in the bar and cross state, respectively. Figures 17(e) and 17(f) compare manual and automatic tuning for the switch's bar state, and Figs. 17(g) and 17(h) compare the two cases for the switch's cross state.

Finally, we repeated the measurement for the bar state stabilization with the data rate of I_1 increased to 25 Gb/s, and its eye diagram at the O_1 port of the switch with the controller stabilizing the switch against an aggressor signal is shown in Fig. 17(i).

The measured eye heights with the controller turned ON vary between 162 mV - 168 mV, which are very similar to the eye heights we reported for the results in the previous section. Furthermore, it can be seen that when the controller is stabilizing the switch against the aggressor signal, the horizontal eye closure is kept minimal, for example, the reader can compare Fig. 13(f) with Fig. 17(f) since both eye diagrams are obtained at the same bit rate, and the horizontal scale in both figures is almost identical.

9. Discussion

Next, we comment on scaling our proposed monitoring approach to large switch fabrics, and compare our work to prior-art.

9.1. Scalability to large switch fabrics

With two 5% optical power taps per switch instead of just one, as illustrated in Fig. 3(a), approximately 0.45 dB of excess loss is incurred per switch due to the two taps. If implemented in a switch fabric described in [18] or [19], with three cascaded switches in each path, the total excess loss will be 1.35 dB. The lower limit to the taps percentages is limited by system-level concerns such as the signal-to-noise ratio (SNR) of the optical signals being tapped, responsivity and noise of the available monitor PDs, and input-referred noise of the electronic circuitry. Lower percentage taps can be used with higher signal SNR and PD responsivity, and lower PD and circuit noise, and vice versa.

In large switch fabrics, the effect of the dissipated power in the MI's phase shifter, and the generated heat therein, on the operating point of the attached switch and nearby switches must be considered. However, since the frequency of the excitation signal to the MI's phase shifter is just 1 kHz in our case, the generated heat fluctuations are outside the thermal bandwidth of the MZI's thermal phase shifters, and hence it would be just an offset to the MZI's normal operating point, and this offset is compensated for by the controller.

9.2. Comparison to published works

Inherent wavelength selectivity in a micro-ring resonator (MRR) filter, combined with the peak in the optical power at its drop port at the desired operating point, is utilized for tuning with a balanced homodyne detection and a PID controller in [20]. A monitoring technique presented in [21] using photoconductive effect also promises low power dissipation and high sensitivity. An MZI-based switch lacks such innate advantages. However, our proposed device does not have elements that need manual tuning, unlike the monitoring devices in [20]- [21].

The approach proposed in [18] for a 1×2 MZI switch is still wavelength indiscriminate and cannot operate on two simultaneous optical signals at different wavelengths. With a sequential approach in the tuning algorithm and the need for a lookup table, the tuning approach in [18] needs to be repeated to account for thermal crosstalk between the switches, to which the design is susceptible due to the small footprint of the device and switch fabric [18]. Our proposed approach does not require a lookup table and can tune a switch fabric in parallel based on the desired state, bar or cross, for each switch unit. Furthermore, our method stabilizes the switch against thermal crosstalk.

Optics EXPRESS

Contactless integrated photonic probes (CLIPPs), whose AC impedance changes based on the presence of optical power in a nearby waveguide, is used in [19] to generate the appropriate monitoring signal, and demonstrate the tuning and stabilization of MZI switches with two optical inputs at different wavelengths. While introducing no optical loss due to monitoring taps, this approach potentially comes at an increase in dissipated electrical power since the CLIPPs need to be excited with an electrical signal with an amplitude of a few volts and frequency in the range 100 kHz - 1 MHz [19]. Most notable, however, is that while our proposed monitoring approach inherently generates the error signal indicative of the switch's state directly from the input signals' wavelengths, the approach in [19] suffers from the penalty of added system complexity represented in the modulation and demodulation of the label signals, which in turn increase linearly with the number of optical inputs to the switch fabric. On the other hand, our proposed device can be operated in a truly digital way with each MZI-MI switch controller needing a single bit that indicates the desired state of that particular switch unit. Finally, the tuning algorithm presented in [19] varies (decreases) the step size to reduce the disturbance to the switch's operating point once a lock condition is detected, which is a useful feature that can easily be added to our tuning algorithm since it would reduce the ripples on the MZI's outputs, such as the ripples on the cross port output in Fig. 16(a), and subsequently reduces potential disturbance to the next switch, as we discussed in section VIII.

10. Conclusion

Large-scale switch fabrics require a 2×2 MZI switch as a building block capable of handling different wavelengths at its inputs. We demonstrate that a secondary monitoring interferometer placed in the MZI switch can be used to indicate the state of the main MZI switch. This monitoring interferometer forms the crucial stage in an active controller that monitors and tunes the main MZI switch to a desired state. The proposed approach can be used to control and stabilize an optical switch matrix that is fully loaded with signals on all inputs.

Funding

Natural Sciences and Engineering Research Council of Canada (NSERC); Huawei Canada; NSERC SiEPIC program.

Acknowledgments

The authors thank CMC Microsystems for providing access to fabrication and design tools, A*STAR IME MPW program for fabrication, S. Nayak, A. Ahmed and A. Sharkia for design help, and Dr. R. Rosales and Mr. R. Mehrabadi for technical support.

References

1. G. T. Reed and A. P. Knights, *Silicon Photonics: An Introduction* (John Wiley & Sons, Ltd, 2004).
2. L. Chrostowski and M. Hochberg, *Silicon Photonics Design: From Devices to Systems* (Cambridge University, 2015).
3. H. Jayatilleka, H. Shoman, R. Boeck, N. A. F. Jaeger, L. Chrostowski, and S. Shekhar, "Automatic configuration and wavelength locking of coupled silicon ring resonators," J. Light. Technol. **36**, 210–218 (2018).
4. L. Chen, E. Hall, L. Theogarajan, and J. Bowers, "Photonic switching for data center applications," IEEE Photon. J. **3**, 834–844 (2011).
5. S. Shekhar, L. Chrostowski, S. Mirabbasi, S. Nayak, M. W. AlTaha, A. Naguib, A. S. Ramani, and H. Jayatilleka, "Silicon electronics-photonics integrated circuits for datacenters," in "IEEE Compound Semiconductor Integ. Circuit Symposium (CSICS)," (2016), pp. 1–4.
6. S. Nakamura, S. Takahashi, I. Ogura, J. Ushida, K. Kurata, T. Hino, H. Takeshita, A. Tajima, M. Yu, and G.-Q. Lo, "High extinction ratio optical switching independently of temperature with silicon photonic 1 x 8 switch," in "Opt. Fiber Comm. Conf. (OFC)," (2012). Paper OTu2I.3.
7. B. G. Lee, A. V. Rylyakov, W. M. J. Green, S. Assefa, C. W. Baks, R. Rimolo-Donadio, D. M. Kuchta, M. H. Khater, T. Barwicz, C. Reinholm, E. Kiewra, S. M. Shank, C. L. Schow, and Y. A. Vlasov, "Monolithic silicon integration of scaled photonic switch fabrics, cmos logic, and device driver circuits," J. Light. Technol. **32**, 743–751 (2014).

Optics EXPRESS

8. D. Celo, D. J. Goodwill, J. Jiang, P. Dumais, C. Zhang, F. Zhao, X. Tu, C. Zhang, S. Yan, J. He, M. Li, W. Liu, Y. Wei, D. Geng, H. Mehrvar, and E. Bernier, "32×32 silicon photonic switch," in "OptoElectronics and Comm. Conf. (OECC)," (2016), pp. WF1–4.
9. L. Qiao, W. Tang, and T. Chu, "32 × 32 silicon electro-optic switch with built-in monitors and balanced-status units," Sci. Reports **7**, 42306 (2017).
10. E. Bernier, P. Dumais, D. J. Goodwill, H. Mehrvar, D. Celo, J. Jiang, C. Zhang, F. Zhao, X. Tu, C. Zhang, S. Yan, J. He, M. Li, W. Liu, Y. Wei, and D. Geng, "Large-scale silicon photonic switch," in "Opt. Fiber Comm. Conf. (OFC)," (2018), p. Th1J.1.
11. M. W. AlTaha, S. Nayak, H. Jayatilleka, S. Shekhar, and S. Mirabbasi, "Silicon-photonic devices: Electronic control and stabilization," in "IEEE Canadian Conf. Electrical and Computer Eng. (CCECE)," (2016), pp. 1–4.
12. F. Morichetti, S. Grillanda, and A. Melloni, "Breakthroughs in photonics 2013: Toward feedback-controlled integrated photonics," IEEE Photon. J. **6**, 1–6 (2014).
13. H. Jayatilleka, K. Murray, M. Ángel Guillén-Torres, M. Caverley, R. Hu, N. A. F. Jaeger, L. Chrostowski, and S. Shekhar, "Wavelength tuning and stabilization of microring-based filters using silicon in-resonator photoconductive heaters," Opt. Express **23**, 25084–25097 (2015).
14. Z. Danyan, H. Guoqiang, H. Xiaohui, and Y. Yang, "Design of an analog maximum power point tracking control IC based on perturb-and-observe algorithm," in "IEEE Int. Conf. Electron Devices and Solid State Circuit (EDSSC)," (2012), pp. 1–4.
15. L. Chen and Y. kai Chen, "Compact, low-loss and low-power 8×8 broadband silicon optical switch," Opt. Express **20**, 18977–18985 (2012).
16. H. Jayatilleka, K. Murray, M. Caverley, N. A. F. Jaeger, L. Chrostowski, and S. Shekhar, "Crosstalk in soi microring resonator-based filters," J. Light. Technol. **34**, 2886–2896 (2016).
17. M. Bahadori, S. Rumley, H. Jayatilleka, K. Murray, N. A. F. Jaeger, L. Chrostowski, S. Shekhar, and K. Bergman, "Crosstalk penalty in microring-based silicon photonic interconnect systems," J. Light. Technol. **34**, 4043–4052 (2016).
18. A. Gazman, E. Manzhosov, C. Browning, M. Bahadori, Y. London, L. Barry, and K. Bergman, "Tapless and topology agnostic calibration solution for silicon photonic switches," Opt. Express **26**, 32662–32674 (2018).
19. A. Annoni, E. Guglielmi, M. Carminati, S. Grillanda, P. Ciccarella, G. Ferrari, M. Sorel, M. J. Strain, M. Sampietro, A. Melloni, and F. Morichetti, "Automated routing and control of silicon photonic switch fabrics," IEEE J. Sel. Top. Quantum Electron. **22**, 169–176 (2016).
20. J. A. Cox, A. L. Lentine, D. C. Trotter, and A. L. Starbuck, "Control of integrated micro-resonator wavelength via balanced homodyne locking," Opt. Express **22**, 11279–11289 (2014).
21. D. Li, L. Zhou, L. Lu, and J. Chen, "Optical power monitoring with ultrahigh sensitivity in silicon waveguides and ring resonators," IEEE Photon. J. **9**, 1–10 (2017).